Large-area fabrication of Au nanoantennas for surface enhanced infrared spectroscopy without an adhesion layer

Lozeman, J. J. A., Srivastava, K., Le-The, H., van den Berg, A., Odijk, M.

J. J. A. Lozeman, K. Srivastava, H. Le-The, A. van den Berg, M. Odijk, "Large-area fabrication of Au nanoantennas for surface enhanced infrared spectroscopy without an adhesion layer," Proc. SPIE 11468, Enhanced Spectroscopies and Nanoimaging 2020, 1146818 (20 August 2020); doi: 10.1117/12.2566757

SPIE.

Event: SPIE Nanoscience + Engineering, 2020, Online Only

Large-area fabrication of Au nanoantennas for surface enhanced infrared spectroscopy without an adhesion layer

J.J.A. Lozeman, K. Srivastava, H. Le-The, A. van den Berg and M. Odijk
BIOS - Lab on a Chip group, MESA+ Institute for Nanotechnology and Max Planck Center for Complex Fluid Dynamics, University of Twente, the Netherlands

ABSTRACT

This work reports the fabrication of large-area Au nanoantennas, tuned to 1400cm^{-1}, on a Si substrate for surface-enhanced-infrared-absorption-spectroscopy. Two different kinds of nanoantennas are fabricated, namely nano-rods and nano-slits. Fabrication is achieved by E-beam lithography (EBL). The need for an adhesion layer is eliminated using our previously reported UV-ozone pre-treatment[1]. To our knowledge, this is the first time this technique is used to fabricate Au nanoantennas on Si without the need adhesion layer, while at the same time obtaining a strong adhesion. This UV-ozone treatment does not only speed up the fabrication process, it can potentially increase the enhancement quality due to the negative influence metallic adhesion layers can have on the plasmon resonance of Au nanoantennas[2–4]. Next to using the standard positive resist for EBL lithography, we also propose a workflow using a negative photoresist to make the nano-rod antennas, potentially speeding up the process by skipping the lift off procedure. Although the negative photoresist fabrication process still requires optimization, our first fabrication attempt show promising results. In order to get the optimal enhancement for a given wavelength, we used FTDT simulations to simulate the structure length, height, width and pitch. After successful simulations, the structures were fabricated and a comparison between the simulated results and fabricated structures was made, confirming the simulation results.

Keywords: SEIRAS, large-area fabrication, Au-nanoantennas, nano-slits, nano-rods, adhesion, FTDT simulations.

1. INTRODUCTION

Infrared (IR) spectroscopy is a powerful analytical technique used in a wide variety of fields such as, the pharmaceutical industry, petroleum industry, feed and food industry, and forensic sciences. With IR spectroscopy, information about the molecular vibrations of a sample can be obtained, which can be translated into the molecular structure of the analyte in question, making IR spectroscopy a strong qualitative technique. Since IR spectroscopy is a spectroscopic technique, the Lambert-Beer law can be applied, allowing the user to obtain not only qualitative, but quantitative information as well. IR spectroscopy is a versatile tool, with operational modes including transmission and reflection spectroscopy, as well as attenuated total reflection (ATR). These different operational modes make it possible for IR spectroscopy to be used on solid, liquid and gaseous samples, giving the technique a wide field of potential applications. Hyphenating IR with separation techniques and secondary detection techniques is also not uncommon, examples are LC-IR, GC-IR, IR-SEC, TG-IR and AFM-IR, enabling even more applications such as the measurements of complex samples. This wide applicability, general ease of use of the instrumentation and the wealth of both quantitative and qualitative information it provides, makes IR spectroscopy a popular technique used in a large number of laboratories around the world.

The one major drawback of IR spectroscopy is the low source power of the instrument. This can cause a low signal to noise (S/N), which limits the user to samples with small cross-sections and requires the instrumentation to operate with expensive, liquid nitrogen cooled detectors to be able to properly detect the lower IR wavelengths. In recent years, two different approaches to increase the S/N have been gaining attention. The first is to increase source power, by for instance, using lasers. The development of QCL lasers has made IR lasers a more affordable option, increasing the peak power of the light source by several orders of magnitude[5]. The second approach, and the focus of this conference proceeding, is by using nanofabricated Au structures to act as antennas for surface-enhanced-infrared-absorption-spectroscopy (SEIRAS).

SEIRAS, first observed by Hartstein *et al.*[6] in the 1980's and further pioneered by the group of Osawa in the 1990's[7,8], is a technique often compared with surface enhanced Raman spectroscopy (SERS), although there are some distinct

Enhanced Spectroscopies and Nanoimaging 2020, edited by Prabhat Verma, Yung Doug Suh, Proc. of SPIE Vol. 11468, 1146818 · © 2020 SPIE
CCC code: 0277-786X/20/$21 · doi: 10.1117/12.2566757

differences. These differences are most notable when comparing the enhancement factors of the two techniques, for SERS[9–11], enhancement factors of up to 10^{10} have been achieved, while reported SEIRAS enhancement factors[12,13] are more modest, in the range of 10^{1-5}. SEIRAS substrates can be roughly categorized in two different groups, namely substrates consisting of roughened metallic films, or so called resonantly tuned nanoantennas. The resonantly tuned nanoantennas, with fine-tuned nanostructured parameters such as the shape, length, width, height and periodicity can provide a higher sensitivity than the roughened metallic films[13]. However, fabrication of these nanoantennas is quite labor-intensive, requiring cleanroom processes and high-resolution nanoscale lithography. The enhancement factor is directly related to the quality and reproducibility of the Au-nanoantennas and for practical applications, large-area fabrication is preferred. Moreover, adhesion of the Au-nanoantennas to Si/SiO_2 substrates is poor and metal adhesion layers like Ti/Cr can affect the plasmonic resonance of the nanoantennas[2–4].

In this work, we present two different nano-antenna designs, nano-rods and nano-slits, based on FTDT simulations. The design of these structures have been reported before in literature, nano-rod antennas have been reported, by amongst others, Huck *et al.*[14,15] and Adato *et al.*[16,17], while nano-slit antennas were first reported by Huck *et al.*[18] The novelty of this work comes with the fabrication of these antennas. Our fabrication technique does not rely on the use of a metallic adhesion layer, simplifying the procedure and potentially improving the enhancement factor. Additionally, we propose a technique to fabricate the Au nano-rods with the use of negative photoresist E-beam lithography (EBL), speeding up the fabrication process by skipping the lift off procedure. As far as the authors are aware, this is the first time that SEIRAS nano-antennas have been fabricated with such a process. We conclude this paper by comparing the fabricated antennas with the simulation results, confirming that the simulations are a valid design tool for future nano-antennas.

2. EXPERIMENTAL

2.1 Simulations

Simulations were performed prior to fabrication in order to determine the structure's optimal shape and array configuration. The simulations were performed by FDTD simulation (Lumerical 2020a Launcher 1.1.2305). Two different nano-antenna designs were simulated, namely nano-rods and nano-slits (see figure 1). The nano-slits designs are the inverse of the nano-rod designs. Several parameters have been varied in order to find the optimal conditions. The parameters varied were: height (h) of the Au layer, the length (l) of the structures, the width (w) of the structures, the pitch between the structures in the x direction (P_x) and the pitch between the structures in the y direction (P_y). The simulations where performed with the following boundary conditions: perfect matched layer (standard) for isolated antennas and periodic boundary conditions in the x and y direction and perfect matched layer in the z direction for the periodic antenna arrays.

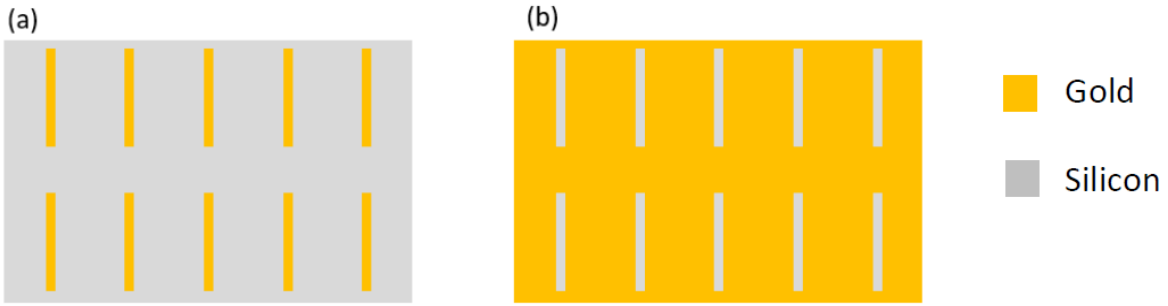

Figure 1: Schematic representation of top view of the nano-antennas. (a) Au nano-rods in a periodic pattern on Si substrate. (b) Au nano-slits in a periodic pattern on a Si substrate.

2.2 Fabrication

Fabrication of the nano-structures was performed in the cleanroom at the MESA$^+$ Institute for Nanotechnology. Three different fabrication processes will be discussed in the next section: the fabrication of the nano-slits and nano-rods using a positive resist and the fabrication of nano-rods using a negative resist.

2.2.1 Nano-slits

In Figure 2, the process flow for the fabrication of the nano-slits is shown. On a Si wafer (one-sided polished (OSP), P-type <100>, 525 µm thick) a thin Au layer of 10 nm was sputtered on the wafer (in-house build sputtering system, pressure: 6.6 x 10^{-3} mbar power: 200 W, deposition rate 41.5 nm/min). Next, the wafer was treated with UV-Ozone for 5 min. (UVP PR-100 UV-Ozone photoreactor) following the procedure described by H. Le-The *et al.*[1] Subsequently, another 40 nm of Au was sputtered to achieve the final structure height of 50 nm. A 255 nm coating of PMMA (NANOtm 950PMMA Series Resists in Chlorobenzene, Organic Polymer Solution. Spin rate: 2500 rpm for 60 s) was spin-coated on the wafer followed by a bake step (180ºC for 120 s). Next, the PMMA was patterned using EBL (Raith EBPG 5150, Raith nanofabrication. Dose: 1400 µC/m^2, beam current: 5 nA), which resulted in a total writing time of 45 min. Following the lithography step, the resist was subsequently developed in a solution of 1:3 MIBK:IPA for 90 s. The excess Au is etched away with ion beam etching (Oxford i300 RIBE, current: 50 mA, voltage: 300 V, accelerator voltage: 500 V). Finally, the remaining resist was stripped away by 99% nitric acid followed by O_2 plasma treatment (Tepla 300, 500 sccm O_2 500 sccm N_2, 800 W, 10 min).

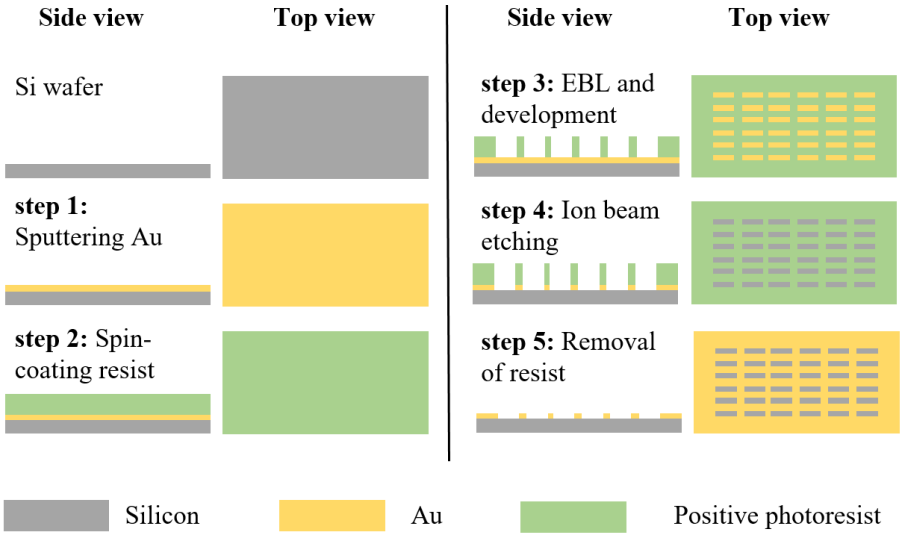

Figure 2: Fabrication process flow Au nano-slits.

2.2.2 Nano-rods (positive resist)

In Figure 3, the process flow describing the fabrication of the nano-rods using positive resist is shown. A silicon wafer (one-sided polished (OSP), P-type <100>, 525 µm thick) was used as a substrate. A 255 nm coating of PMMA (NANO^{tm} 950PMMA Series Resists in Chlorobenzene, Organic Polymer Solution. Spin rate: 2500 rpm for 60 s) was spin-coated on the wafer followed by a bake step (180ºC for 120 s). Next, the PMMA was patterned using EBL (Raith EBPG 5150, Raith nanofabrication. Dose: 1400 µC/m^2, beam current: 5 nA), which resulted in a total writing time of 45 min. After the lithography procedure, the resist was developed in a solution of 1:3 MIBK:IPA for 90 s. Following the successful development, 10 nm of Au was sputtered on the wafer (in-house build sputtering system pressure: 6.6 x 10^{-3} mbar power: 200 W, deposition rate 41.5 nm/min). Next, the wafer was treated with UV-Ozone for 5 min. (UVP PR-100 UV-Ozone photoreactor). Subsequently another 40nm of Au was sputtered to achieve the final structure height of 50 nm. Finally, the wafer was submerged in a beaker of 99% nitric acid till lift off was completed in order to remove the photoresist and excess Au material.

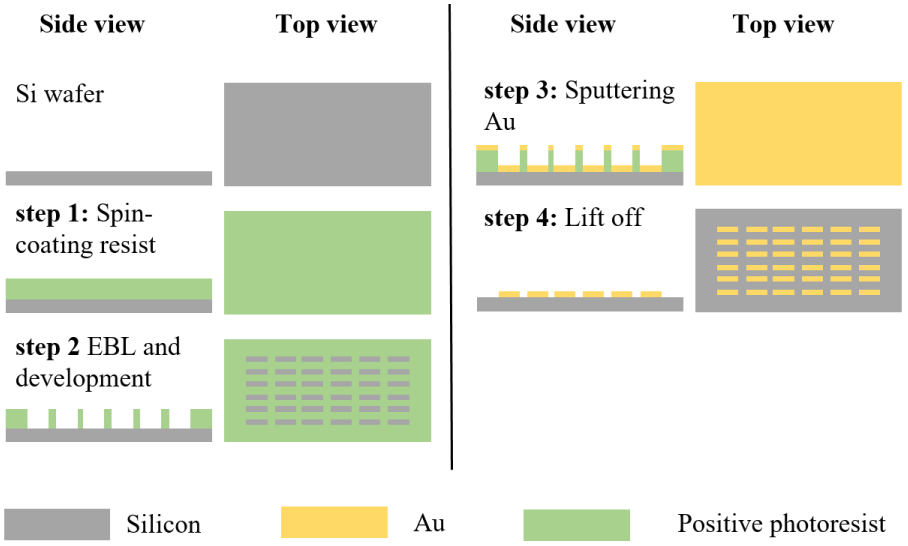

Figure 3: Fabrication process flow for the nano-rods using a positive photoresist

2.2.3 Nano-rods (negative resist)

Figure 4 describes the process flow of the fabrication of the nano-rods using negative resist. On a silicon wafer (one-sided polished (OSP), P-type <100>, 525 µm thick) a thin Au layer of 10 nm was sputtered onto the wafer (In-house build sputtering system pressure: 6.6 x 10^{-3} mbar power: 200 W, deposition rate 41.5 nm/min). Next, the wafer was treated with UV-Ozone for 5 min. (UVP PR-100 UV-Ozone photoreactor). In order to complete the Au-layer, another 40 nm of Au was sputtered to achieve the final structure height of 50 nm. A 400 nm coating of AR-n7520 (Allresist GmbH. Spin rate: 4000 rpm for 60 s) was spin-coated on the wafer followed by a bake step (85ºC for 60 s). Next, the negative resist was patterned using EBL (Raith EBPG 5150, Raith nanofabrication. Dose: 1900 µC/m^2, beam current: 5 nA). Subsequently, the resist was developed in a solution of AR-300:47 (Allresist GmbH) for 90 s. The excess Au is etched away with ion beam etching (Oxford i300 RIBE, current: 50 mA, voltage: 300 V, accelerator voltage: 500 V). Finally, the remaining resist was stripped away by 99% nitric acid followed by O_2 plasma treatment (Tepla 300, 500 sccm O_2 500 sccm N_2, 800 W, 20 min).

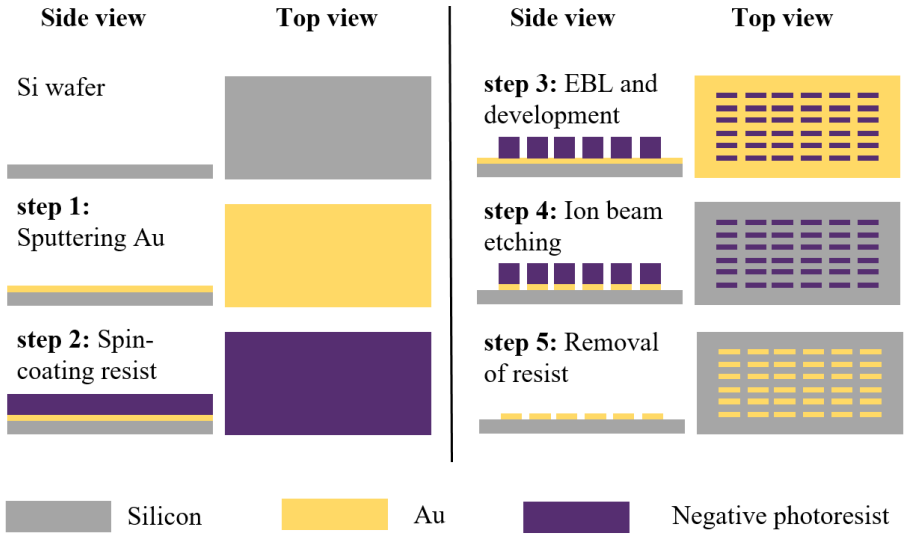

Figure 4: Fabrication process flow for the nano-rods using positive photoresist

2.3 Measurements

Measurement of a wafer containing the nano-antennas has been performed using a Bruker vertex 70v. The large area nanoantennas were aligned with the IR-beam using an in-house build aligner, containing polarization filter. Measurements were performed in transmission mode. Due to global pandemic events and resulting lock-down, only one sample was able to be measured.

3. RESULTS AND DISCUSSION

3.1 Simulations results

In Figure 5 the simulation results of a nano-rod and nano-slit are shown. As can be seen in these figures, when the structures are excited with polarized light ($E_{parallel}$ for the nano-rods and $E_{perpendicular}$ for the nano-slits) resonant accumulation of the charges occurs, acting as hot spots for SEIRAS. The accumulations of the charges occurs at the edges of the nano-rods while in the nano-slits the accumulation appears in the center of the slits. These results correspond with literature, as shown by Huck *et al.*[18]

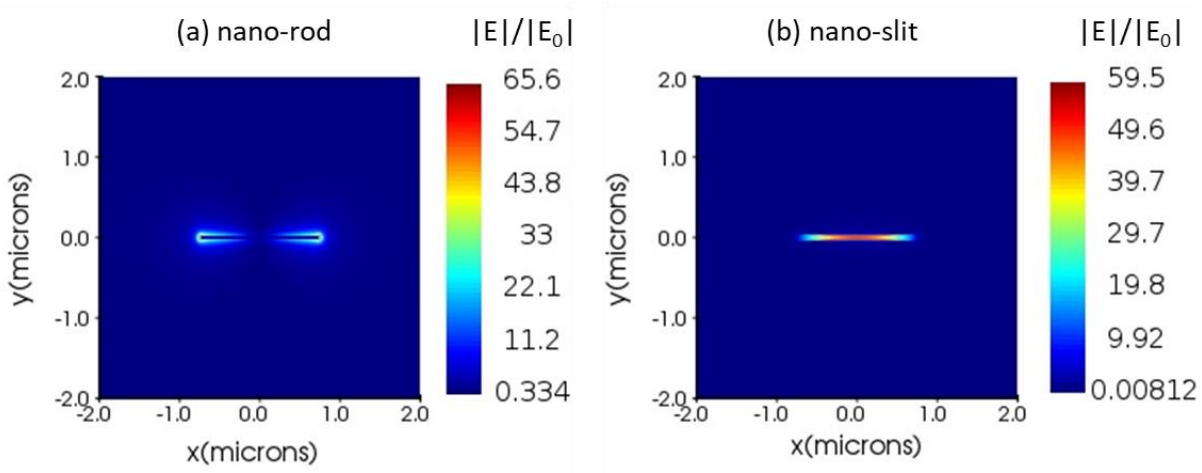

Figure 5: Simulation results showing normalized electric field density for the Au nano-antennas (a) Nano-rod structure with the dimensions l: 1500 nm, w: 50 nm, h: 50 nm. The nano-rods are excited with parallel polarized light .(b) Nano-slit structure with the dimensions l: 1500 nm, w: 50 nm, h: 50 nm. The nano-slits are excited with perpendicular polarized light

As is clear from Figure 6a, the length of an antenna is critical in order to determine the frequency at which the enhancement takes place. As can be seen from this figure, when the length of an antenna is increased, the wavelength where resonance occurs also increases. These results show high agreement with existing literature[14]. For a given length of an antenna, the height and width were varied in order to gain a maximum enhancement. It was found that the optimal width and height for the nanoantennas was in a range of 50-150 nm in width and 50-150 nm in height. Next, the periodicity between the antennas was investigated by varying the distance between the antennas in the P_y direction and P_x direction. Periodicity is measured as the distance from the center of one antenna to the center of its neighboring antenna. A change in enhancement can be observed due to the so called far-field coupling of the antennas[19]. In figure 6b, one example of the optimal periodicity between antennas with a size of l: 1500 nm w: 50 nm h: 50 nm, is studied. First, the periodicity for P_x is set to 4 µm, while the P_y is varied, as can be seen in the figure, the optimal signal is obtained at an P_y of 3 µm. Next, P_y is set to 3 µm while P_x is varied, resulting in an optimal value at 4.2 µm.

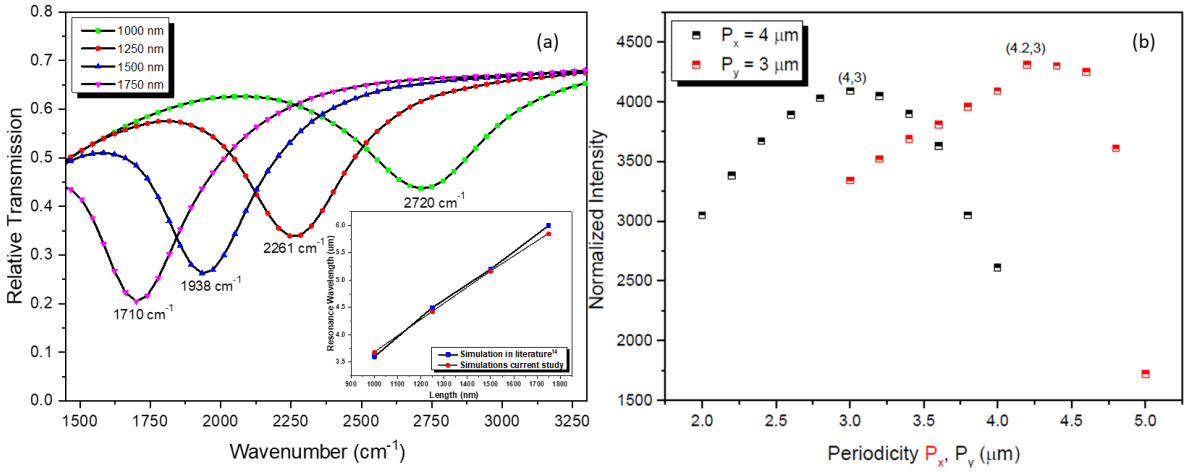

Figure 6: Optimizing antenna dimensions. The figures shown have the dimensions of h: 50 nm, w: 50 nm (a) varying the length of the antennas will change the enhancement frequency. The simulations are in agreement with literature[14]. (b) by varying the pitch between antennas with a given length, a maximum enhancement intensity can be determined. Shown are antennas with a length of 1500 nm. Plotted in black are antennas with a P_x of 4 µm, while varying the P_y obtaining a maximum enhancement at a P_y of 3 µm. Plotted in red are antennas with a P_y of 3 µm, while varying the P_x a maximum enhancement intensity is found at a P_x of 4.2 µm, resulting in an optimal enhancement for antennas with these particular dimension when using a periodicity of P_x of 4.2 µm and a P_y of 3 µm.

3.2 Fabrication results

3.2.1 Positive resist fabrication

In Figure 7, the fabrication results of some of the fabricated nano-antennas are shown. Figures 7a and 7b show the nano-slits and nano-rods, fabricated with the positive photoresist, respectively. The quality of the antennas look as expected, the slits and rods have straight walls and sharp corners and show little defects. The dimensions show some variations compared to the designs, which is most significant for the width of the structures. For instance, the width of the slits shown in figure 7a is measured to be 90 nm, while being designed to be 70 nm, additionally, the width for the rods in Figure 7b is measured to be 180 nm, while being designed to be 230 nm. This is probably caused by the beam size during the EBL process and could be improved by optimizing the procedure.

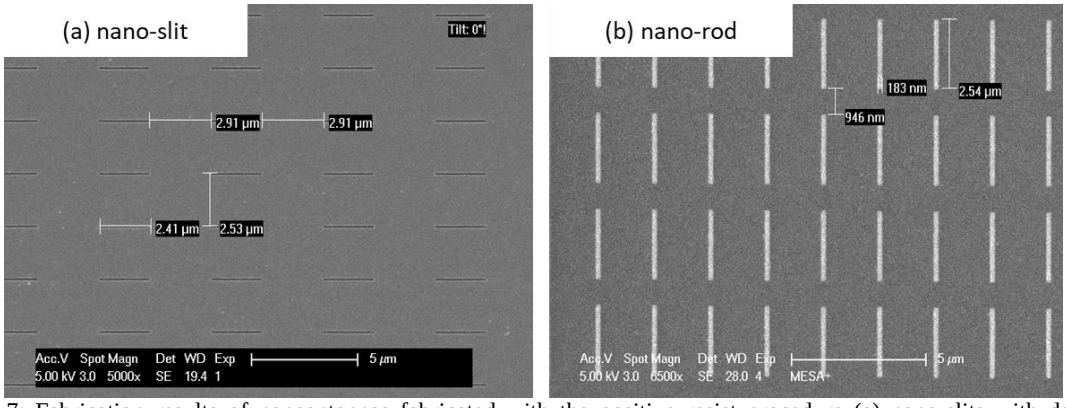

Figure 7: Fabrication results of nanoantennas fabricated with the positive resist procedure (a) nano-slits with designed dimensions l: 2500 nm w: 70 nm measured dimension: l: 2410 nm w: 90 nm. (b) nano-rods with designed dimensions l: 2500 nm w: 230 nm measured dimension: l: 2540 nm w: 180 nm.

3.2.2 Negative resist fabrication

More interesting are the nano-rods fabricated by the negative photoresist procedure. In Figure 8a and 8b, the first results of the negative resist nano-rods are shown. These gold rods show a deviation of the design, most notably it shows sharp spiky features on the Au rods and a wide variety in the width of the structures. These spiky features are possibly a result of the negative resists cross linking and can be improved by optimizing the procedure. Although roughness is usually attributed to be a beneficial contribution to surface enhancement, roughness in this size is probably detrimental for the enhancement.

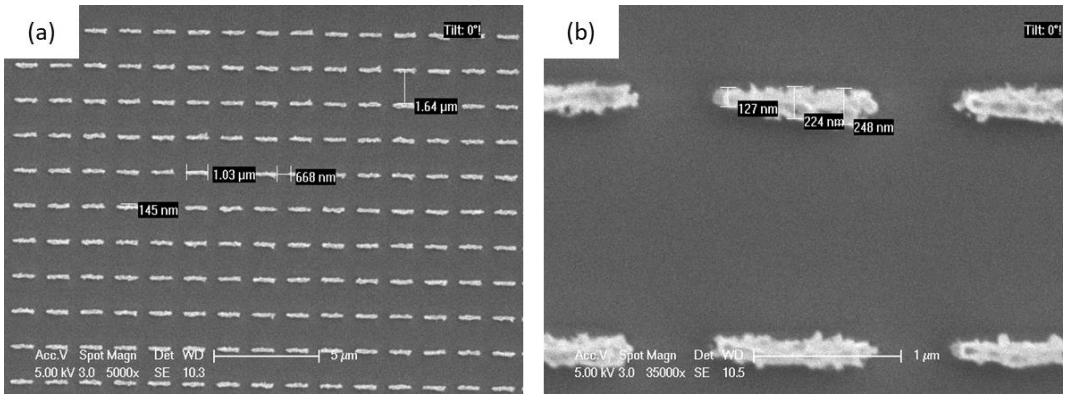

Figure 8: Fabrication results of nano-rod antennas fabricated with the negative resist procedure (a) nano-rods with designed dimensions l: 1000 nm w: 70 nm measured dimension: l: 1000 nm w: 130-250 nm. (b) zoomed in image of the nano-rods shown in figure 8a

3.3 Measurements results

In Figure 9, the simulation and experimental results of an array of gold nano-rods with the dimensions of l: 1100 nm, w: 230 nm h: 50 nm P_x: 2600 nm P_y: 2400 nm, fabricated using the positive resist procedure, are shown. As can be seen in this figure, the absorption peak of the measured structures (1360cm^{-1}) is at a comparable frequency as the simulated results (1367cm^{-1}). A small dip in the signal at 1250 cm^{-1} can be seen in the experimental results. This dip is probably caused by contaminant on the wafer

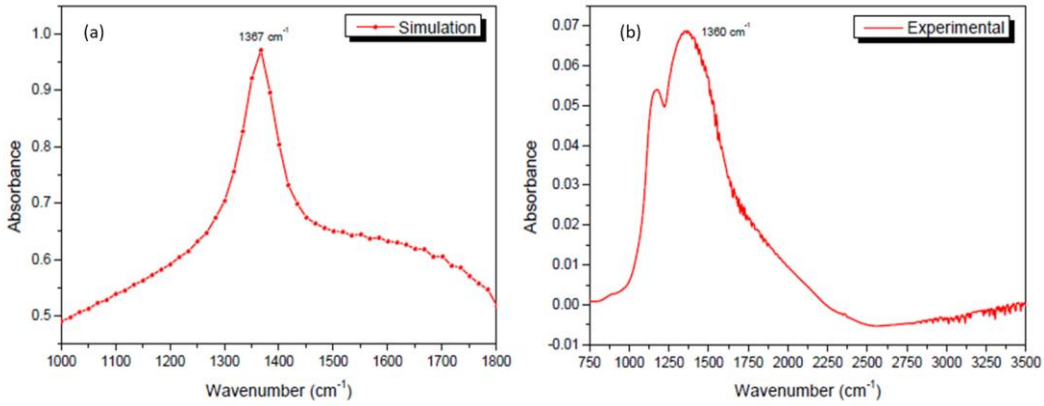

Figure 9: Nano-rod antenna with the dimensions of l: 1100 nm, w: 230 nm h: 50 nm Px: 2600 nm Py: 2400 nm. (a) simulation results (b) experimental results.

4. CONCLUSION

We show that the new fabrication technique to improve the Au adhesion to Si by using the UV-ozone treatment works for the fabrication of Au nano-rod and nano-slit antennas. This UV-ozone treatment removes the need for a metallic adhesion layers for the fabrication of Au nanostructures on Si substrates, which not only simplifies the fabrication process, but the absence of a metallic adhesion layer can also improve the enhancement factor. Next to the UV-ozone

treatment, we report on a novel EBL procedure to fabricate gold nano-antennas by the use of negative photoresist, which can speed up the fabrication process of Au nano-rod antennas by skipping the lift off procedure. Although optimization of the procedure is required, these first results show significant promise. Finally we show the measurement result of one of the fabricated nano-rod antennas and compared it with the simulation results, which are in agreement.

ACKNOWLEDGEMENTS

This work was supported by the Netherlands Center for Multiscale Catalytic Energy Conversion (MCEC), and the Netherlands Organisation for Scientific Research (NWO) Gravitation programme funded by the Ministry of Education, Culture and Science of the government of the Netherlands.

REFERENCES

1. Le-The, H. *et al.* Postdeposition UV-Ozone Treatment: An Enabling Technique to Enhance the Direct Adhesion of Gold Thin Films to Oxidized Silicon. *ACS Nano* **13**, 6782–6789 (2019).
2. Debu, D. T., Ghosh, P. K., French, D. & Herzog, J. B. Surface plasmon damping effects due to Ti adhesion layer in individual gold nanodisks. *Opt. Mater. Express* **7**, 73 (2017).
3. Jiao, X., Goeckeritz, J., Blair, S. & Oldham, M. Localization of near-field resonances in bowtie antennae: Influence of adhesion layers. *Plasmonics* **4**, 37–50 (2009).
4. Huang, J. S. *et al.* Atomically flat single-crystalline gold nanostructures for plasmonic nanocircuitry. *Nat. Commun.* **1**, 1–8 (2010).
5. Weida, M. J. & Yee, B. Quantum cascade laser-based replacement for FTIR microscopy. in *Imaging, Manipulation, and Analysis of Biomolecules, Cells, and Tissues IX* (eds. Farkas, D. L., Nicolau, D. V. & Leif, R. C.) **7902**, 79021C (2011).
6. Hartstein, A., Kirtley, J. R. & Tsang, J. C. Enhancement of the infrared absorption from molecular monolayers with thin metal overlayers. *Phys. Rev. Lett.* **45**, 201–204 (1980).
7. Osawa, M., Ataka, K. ichi, Yoshii, K. & Yotsuyanagi, T. Surface-enhanced infrared ATR spectroscopy for in situ studies of electrode/electrolyte interfaces. *J. Electron Spectros. Relat. Phenomena* **64**–**65**, 371–379 (1993).
8. Ataka, K. I., Yotsuyanagi, T. & Osawa, M. Potential-dependent reorientation of water molecules at an electrode/electrolyte interface studied by surface-enhanced infrared absorption spectroscopy. *J. Phys. Chem.* **100**, 10664–10672 (1996).
9. Le-The, H. *et al.* Wafer-scale fabrication of high-quality tunable gold nanogap arrays for surface-enhanced Raman scattering. *Nanoscale* **11**, 12152–12160 (2019).
10. Lozeman, J. J. A., Führer, P., Olthuis, W. & Odijk, M. Spectroelectrochemistry, the future of visualizing electrode processes by hyphenating electrochemistry with spectroscopic techniques. *Analyst* **145**, 2482–2509 (2020).
11. Ru, E. C. Le & Etchegoin, P. G. *Principles of Surface-Enhanced Raman Spectroscopy*. (Elsevier, 2009). doi:10.1016/B978-0-444-52779-0.X0001-3
12. Ataka, K. & Heberle, J. Biochemical applications of surface-enhanced infrared absorption spectroscopy. *Anal. Bioanal. Chem.* **388**, 47–54 (2007).
13. Kühner, L. *et al.* Nanoantenna-Enhanced Infrared Spectroscopic Chemical Imaging. *ACS Sensors* **2**, 655–662 (2017).
14. Huck, C. *et al.* Gold Nanoantennas on a Pedestal for Plasmonic Enhancement in the Infrared. *ACS Photonics* **2**, 497–505 (2015).
15. Huck, C. *et al.* Surface-Enhanced Infrared Spectroscopy Using Nanometer-Sized Gaps. *ACS Nano* **8**, 4908–4914 (2014).
16. Adato, R., Aksu, S. & Altug, H. Engineering mid-infrared nanoantennas for surface enhanced infrared absorption spectroscopy. *Biochem. Pharmacol.* **18**, 436–446 (2015).
17. Adato, R. *et al.* Ultra-sensitive vibrational spectroscopy of protein monolayers with plasmonic nanoantenna arrays. *Proc. Natl. Acad. Sci.* **106**, 19227–19232 (2009).
18. Huck, C. *et al.* Plasmonic Enhancement of Infrared Vibrational Signals: Nanoslits versus Nanorods. *ACS Photonics* **2**, 1489–1497 (2015).
19. Bagheri, S. *et al.* Fabrication of Square-Centimeter Plasmonic Nanoantenna Arrays by Femtosecond Direct Laser Writing Lithography/ Effects of Collective Excitations on SEIRA Enhancement. *ACS Photonics* **2**, 779–786 (2015).